Analysis of the regional ionosphere at low latitudes in support of the Biomass ESA mission

L. Alfonsi, G. Povero, L. Spogli, C. Cesaroni, B. Forte, C. N. Mitchell, R. Burston, S. Veettil, M. Aquino, V. Klausner, M. T. A. H. Muella, M. Pezzopane, A. Giuntini, I. Hunstad, G. De Franceschi, E. Musicò, M. Pini, V. La The, H. Tran Trung, A. Husin, S. Ekawati, C. V. de la Cruz-Cayapan, M. Abdullah, N. Mat Daud, M. Le Huy, N. Floury

***Abstract*— Biomass is a spaceborn polarimetric P-band (435 MHz) synthetic aperture radar (SAR) in a dawn-dusk low Earth orbit. Its principal objective is to measure biomass content and change in all the Earth's forests. The ionosphere introduces Faraday rotation on every pulse emitted by low-frequency SAR and scintillations when the pulse traverses a region of plasma irregularities, consequently impacting the quality of the imaging. Some of these effects are due to Total Electron Content (TEC) and its gradients along the propagation path. Therefore, an accurate assessment of the ionospheric morphology and dynamics is necessary to properly understand the impact on image quality, especially in the equatorial and tropical regions. To this scope, we have conducted an in-depth investigation of the significant noise budget introduced by the two crests of the Equatorial Ionospheric Anomaly (EIA) over Brazil and South-East Asia. The work is characterized by a novel approach to conceive a SAR-oriented ionospheric assessment, aimed at detecting and identifying spatial and temporal TEC gradients, including scintillation effects and Traveling Ionospheric Disturbances, by means of Global Navigation Satellite Systems (GNSS) ground-based monitoring stations. The novelty of this approach resides in the customization of the information about the impact of the ionosphere on SAR imaging as derived by local dense networks of ground instruments operating during the passes of Biomass spacecraft. The results identify the EIA crests as the regions hosting the bulk of irregularities potentially causing degradation on SAR imaging. Interesting insights about the local characteristics of low-latitudes ionosphere are also highlighted.**

***Index Terms*—Equatorial Ionospheric Anomaly, Ionospheric impact on Synthetic Aperture Radar, ionospheric climatology, TEC gradients**

I. Introduction

The Biomass mission is envisaged to be launched around 2021 and it is planned to cover a five-year duration. The space segment consists of a single satellite in a near-polar, Sun-synchronous orbit at an altitude of 637–666 km. The orbit is designed to enable repeat pass interferometric acquisitions throughout the mission's lifetime and to minimise the impact of disturbances from the ionosphere [1]. Nevertheless, given the radar working frequency (435 MHz) and the disturbed nature of the low-latitude ionosphere, some special care is being given to the potential corruption that the ionosphere can induce on Synthetic Aperture Radar (SAR) imaging.

The ionosphere can introduce several effects into the Biomass SAR imaging process, such as:

1. Cross-talk caused by Faraday rotation;
2. Loss of spatial resolution caused by scintillation
3. Azimuthal image shifts caused by TEC spatial gradients.

These effects are determined by the Total Electron Content (TEC) along the propagation path of every pulse emitted by the

This study has been funded by the European Space Agency under the Alcantara initiative of the General Study Programme through two projects: IRIS - Ionospheric Research for Biomass in South America (ESA Contract No. 4000117287/16/F/MOS) and IBisCo - Ionospheric environment characterization for Biomass Calibration over South East Asia (ESA Contract no. 4000117285/16/F/MOS).

Cathryn Mitchell also acknowledges support from the UK NERC NE/P006450/1.

Lucilla Alfonsi, Luca Spogli, Claudio Cesaroni, Michael Pezzopane, Alessandra Giuntini, Ingrid Hunstad, Giorgiana De Franceschi, and Elvira Musicò are with the Istituto Nazionale di Geofisica e Vulcanologia, Roma, Italy (e-mail: {*name.surname*}@ingv.it).

Gabriella Povero and Marco Pini are with the Istituto Superiore Mario Boella, Torino, Italy (e-mail: {*surname*}@ismb.it).

Biagio Forte, Robert Burston and Cathryn N. Mitchell are with the University of Bath, UK (e-mail: {b.forte, rjb22, c.n.mitchell}@bath.ac.uk).

Sreeja Veettil, and Marcio Aquino are with the University of Nottingham, UK (e-mail: {*name.surname*}@nottingham.ac.uk).

Virginia Klausner and Marcio Muella are with the Universidade do Vale do Paraíba (UNIVAP), Instituto de Pesquisa e Desenvolvimento (IP&D), Brazil (e-mail: {virginia, mmuella}@univap.br).

La The Vinh and Tran Trung Hieu are with the Hanoi University of Science and Technology, Hanoi, Vietnam (email: {vinh.lathe, hieu.trantrung-navis} @hust.edu.vn).

Asnawi Husin and Sri Ekawati are with the National Institute of Aeronautics and Space (LAPAN), Indonesia (e-mail: {asnawi, sri.ekawati}@lapan.go.id).

Charisma V. de la Cruz.Cayapan is with the National Mapping and Resource Information Authority (NAMRIA), The Philippines (e-mail: cvdcayapan@namria.gov.ph).

Mardina Abdullh and Noridawaty Mat Daud are with the Universiti Kebangsaan Malaysia (UKM), Malaysia (e-mail: {mardina, nmd}@ ukm.edu.my).

Minh Le Huy is with the Institute of Geophysics, Vietnam Academy of Science and Technology, Vietnam (e-mail: lhminhigp@gmail.com).

Nicolas Floury is with the European Space Agency, Noordwijk, The Netherlands (e-mail: nicolas.fleury@esa.int).

Luca Spogli is also collaborating with SpacEarth Technology, Roma, Italy.

Elivira Musicò is also a PhD student at University "Sapienza" of Rome, Italy.

SAR. The slant TEC derived from GNSS signals received by ground receivers is a physical quantity, which provides the number of free electrons over 1 m^2 cross-sectional along the ray path connecting receiver and satellite. As the bulk of free electrons is in the ionosphere, a good knowledge of the local features of the equatorial and low-latitude ionosphere can help in optimising Biomass performance and in decision making such as for the choice of external calibration sites [2]. This is one of the reasons that triggered ESA to support, at the end of 2015, studies of the upper atmosphere through the Alcantara initiative of the General Studies Programme (https://gsp.esa.int/alcantara). Two projects, named IRIS (Ionospheric Research for Biomass in South America) and IBisCo (Ionospheric environment characterization for Biomass Calibration over South East Asia), were among the successful proposals. IRIS and IBISCO released an in-depth climatological description of the Brazilian as well as the Southeast Asian Equatorial Ionospheric Anomaly (EIA) used to support Biomass-related investigations. The main objective of this paper is to report the principal findings of the two projects, highlighting the original approach adopted to assess the regional characteristics of TEC, TEC gradients and scintillations around 06 AM and 06 PM local times of the Biomass orbital passes.

The low-latitude ionosphere is characterized by electron density gradients, termed as blobs and bubbles, which are signatures of the inhomogeneous distribution of the free electrons resulting from the complex electrodynamics featuring in the region [3]. The daytime equatorial ionosphere presents northward and eastward electric fields generated in the E region that are mapped along the magnetic field lines to F-region. These electric fields depend strongly on magnetic flux-tube integrated conductivity. The joint action of magnetic field (B) and zonal electric field (E) causes an ExB drift that moves plasma upward during day. The uplifted plasma then, under the action of the gravitational force, diffuses to higher latitudes, and two electron density-enhanced regions, defined as “equatorial ionization anomaly (EIA) crests”, appear in both the northern and southern ±15°/±20° low-latitude magnetic sectors, leaving a trough at the magnetic equator. This phenomenon is known as the “fountain effect” and gives rise to the EIA [3], [4], [5]. It is worth highlighting that besides the ExB drift and field-aligned diffusion of plasma, meridional winds modulate the morphology of the EIA, whose crests are raised in the windward hemisphere by trans-equatorial meridional winds through the ion drag effect (e.g. [6]). After the local sunset, the low-latitude ionosphere presents also an additional peculiar feature: the prereversal enhancement (PRE) [7]. PRE is superimposed to the daytime upward and nightime downward drift of plasma, creating the condition for a destabilization of the ionosphere due to the Rayleigh-Taylor Instability [8]. Such condition favours the formation of irregularities of several scale sizes resulting in TEC gradients, scintillations and equatorial spread F (ESF) (presence of electron density irregularities visible as diffuse echoes on the ionograms at F altitude) [9]. Scintillations appear as phase and amplitude fluctuations of the trans-ionospheric signals received at ground. Ionospheric changes can be even more dramatic during magnetic storms [10].

The choice to design the Biomass mission with the orbital passes at 06 AM and 06 PM could save the SAR imaging from the ionospheric perturbation occurring mainly in the evening hours. Nevertheless, some degradation could also be observed in the 06 PM pass because of the ionospheric instability about to happen in the succeeding hours.

The coupling between ionized and neutral atmosphere can also result in the formation of Traveling Ionospheric Disturbances (TIDs). TIDs are the ionospheric manifestation of gravity waves propagating in the neutral atmosphere [11]. These disturbances are one of the most common ionospheric phenomena that can contribute to TEC perturbations. TIDs are classified into two main categories, namely large-scale TIDs (LSTIDs) with a period greater than 1 hour and moving faster than 0.3 km/s, and medium-scale TIDs (MSTIDs) with shorter periods (from 10 min to 1 hour) and moving more slowly (0.05–0.3 km/s) ([12] and the references therein). The origin of MSTIDs is usually attributed to the neutral atmospheric turbulence associated with meteorological activity or to the vertical irradiance gradient associated with the solar terminator ([12] and the references therein).

The occurrence of external perturbations originating from the Sun and affecting the magnetosphere-ionosphere coupling makes the EIA configuration very different from the one assumed during quiet times. In particular, the EIA crests can disappear, causing the suppression of the ionospheric irregularities producing scintillations. In other cases, the disturbances can intensify the EIA resulting in the exacerbation of scintillations and LSTIDs occurrence [13], [14]. During the same storm, inhibition and intensification of the ionospheric scintillations can concur (see, e.g., [15]).

This paper focuses on the description of the ionospheric climatology derived from TEC and GNSS scintillation data acquired in the years 2014 and 2015 in Brazil and Southeast Asia under quiet geomagnetic conditions. The second section focuses on the data used for the analysis, while the third section describes the original approach adopted to highlight the behaviour shown by the low-latitude ionosphere at the different observed longitudinal sectors. The fourth section describes and discusses the achieved results. Since results for South East Asia (SEA) and Brazil present peculiar characteristics, they are described separately. Differences and similarities found in the ionospheric environment of the two regions are reported in the concluding remarks.

II. Data

The ionospheric irregularities appearing as steep TEC gradients describe the inhomogeneous distribution of free electrons in the upper atmosphere. Since TEC is an intrinsic characteristic of the ionosphere, it is independent of the working frequency used to probe the plasma. Differently, as scintillation is an effect induced on the amplitude and phase of the signal, its measurement is frequency dependent. This means that the use of GNSS data can provide a complete TEC scenario but can only give a partial description of scintillation climatology at the P-band (Biomass working frequency). At

low latitudes, the worst scintillation effects occur on the amplitude of the signals. The amplitude fluctuations are mainly caused by ionospheric irregularities with sizes of the order of the first Fresnel zone, which at the (GNSS signals) L-band corresponds to scales of hundreds of meters, while at the P-band corresponds to scales of kilometres. This implies that the L-band scintillation climatology addresses ionospheric irregularities of one order of magnitude smaller than those causing P-band scintillation [16], [17]. Unfortunately, a long-term coverage of P-band measurements of the ionosphere is not available, so the climatology of scintillation to support Biomass presented here is derived from GNSS data. Nevertheless, an in-depth study of TEC gradients can give important insights on the ionospheric morphology and, in particular, on the different scale-sizes of the electron density structures present in the upper atmosphere. Further information can be inferred by the comparison between TEC and the L-band scintillation climatology.

A. Data providers and instrumentation

In SEA, the institutions providing the data are: Institute of GeoPhysics of the Vietnamese Academy of Science and Technology – VAST-IGP (Vietnam), Universiti Kebangsaan Malaysia - UKM (Malaysia), National Institute of Aeronautics and Space of Indonesia - LAPAN (Indonesia) and National Mapping and Resource Information Authority - NAMRIA (The Philippines). Such institutions provided RINEX and scintillation data from the stations shown in Figure 1. The Southeast Asian region is dived in two sub regions, West and East SEA, with respect to the 115°E meridian.

In South America, in terms of GNSS receivers, the largest network is the Brazilian Network for Continuous GNSS Monitoring (RBMC), managed by the Department of Geodesy of the Brazilian Institute of Geography and Statistics (IBGE). The stations of the RBMC/IBGE integrate the Reference Network SIRGAS (Geocentric Reference System for the Americas). Data from more than 100 GNSS receivers are available under request from the IBGE website (http://www.ibge.gov.br). The Brazilian Space Weather Program (EMBRACE), managed by the National Institute for Space Research INPE, uses data from RBMC/IBGE to provide TEC products for the technical and scientific communities. A second network of GNSS receivers managed by INPE under the EMBRACE program is available only for scintillation monitoring. Some of these receivers are also part of the permanent array of instruments from the Low-Latitude Ionospheric Sensor Network (LISN). The EMBRACE/INPE network consists of 17 GNSS receivers, however only 6 scintillation monitors have recently been in operation (http://www2.inpe.br/climaespacial/portal/sci-home/). A third network is part of a joint collaboration between the São Paulo State University (UNESP), INPE and Universidade do Vale do Paraiba (UNIVAP). This network was established as result of the CIGALA and CALIBRA projects (EU/GSA FP7). Although the CIGALA/CALIBRA network can also provide dual-frequency data for TEC investigations, this network was deployed mainly for continuous monitoring of ionospheric scintillations over Brazil. Presently, 10 GNSS receivers for scintillation monitoring are in operation in the CIGALA/CALIBRA network (http://is-cigala-calibra.fct.unesp.br/is/). The sites providing data in Brazil are described in Figure 2. In the same figure, the red and green boxes indicate the geographic sectors considered for the characterization of the geomagnetic equator (red) and crest (green) regions, respectively.

III. METHOD

To assess the climatology of the ionosphere we based our analysis on two quietest days provided for each month by the World Data Center for Geomagnetism, Kyoto (http://wdc.kugi.kyoto-u.ac.jp/qddays/index.html) between March 2015 and February 2016 for SEA region and along the entire 2015 for Brazil. These periods have been selected to ensure a good data coverage and at the same time taking advantage of the data acquired during the ERICA campaign conducted in South East Asia [15], [18].

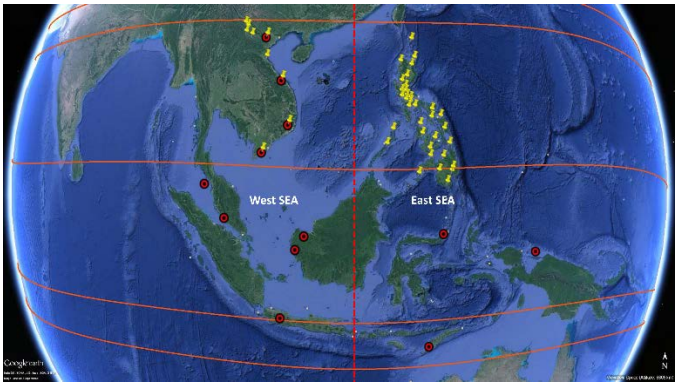

Fig. 1. Location of the GNSS stations (geodetic receivers: pins; scintillation receivers: circles). Orange lines represent the expected position of the geomagnetic equator and the isoclinic lines at magnetic latitude of ± 15° and ±20°. Red dashed line indicates the meridian at 115°E.

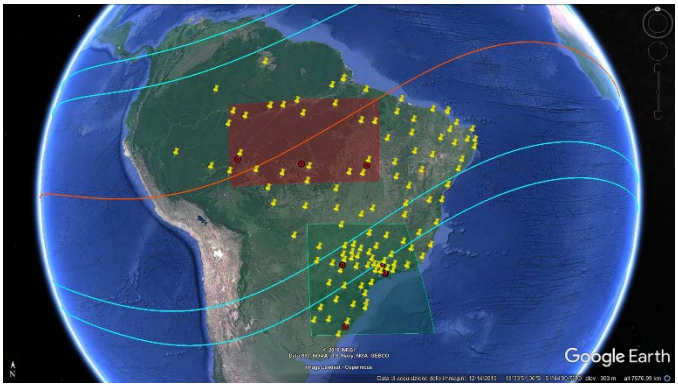

Fig. 2. Location of the GNSS receivers of the RBMC network (yellow pins) used for the TEC analysis and of the GNSS receivers of the LISN and CIGALA (red circles) used for scintillation analysis. The red and green boxes indicate the geographic sector considered for the characterization of the geomagnetic equator (red) and crest regions (green), respectively. The orange line represents the expected position of the geomagnetic equator, while cyan lines indicate the isoclinic lines at magnetic latitude of ± 15° and ±20°.

The two quietest days of each month allow the definition of an "average" undisturbed ionosphere, useful to describe the main

features of interest for Biomass, which is foreseen to be launched under solar minimum conditions (2021) and to remain in orbit during the ascending period of the next solar cycle. Special focus is given to the times of the foreseen Biomass orbital passes, i.e. local 06 AM and 06 PM. In particular, the monthly variation of TEC and TEC gradients have been derived considering a 1-hour window centred around 06 AM and 06 PM.

The ionospheric assessment has been investigated through the study of TEC (including its spatial and temporal variation) and amplitude scintillation (S4).

A. TEC and TEC gradients determination

TEC values are retrieved by using GPS phase and code measurements on L1 and L2. In order to cancel out satellite and receiver inter-frequency biases, the calibration technique described in [19] and further detailed in [20] was applied. To obtain maps of TEC over regions of interest, the "natural neighbour" interpolation technique has been applied. According to [21], in the case of local maps of TEC, this technique gives better results than other commonly used methods, such as linear, inverse distance weighting, Kriging, etc. The natural neighbour interpolation technique is based on the identification of the Voronoi cell associated with a set of scattered points in the selected area [22]. The Voronoi polygons network can be constructed through Delauney triangulation of the data [23].

The TEC spatial gradients have been derived from the TEC maps produced with the previously described method. In particular, we have calculated the TEC gradients along both the North-South direction ΔTEC_{N-S} and the East-West direction ΔTEC_{E-W} with the following equation [20]:

$$\Delta TEC_{N-S}\left(GP_{i,j}\right) = \frac{TEC\left(GP_{i+1,j}\right) - TEC\left(GP_{i,j}\right)}{d_i} \quad (1)$$

$$\Delta TEC_{E-W}\left(GP_{i,j}\right) = \frac{TEC\left(GP_{i,j+1}\right) - TEC\left(GP_{i,j}\right)}{d_j} \quad (2)$$

Where $\Delta TEC_{N-S}\left(GP_{i,j}\right)$ is the TEC gradient along the North-South direction calculated for the point of the grid with coordinates *(i,j)*, $TEC\left(GP_{i+1,j}\right)$ is the TEC value of the first northerly point of the grid with respect to *(i,j)*, $TEC\left(GP_{i,j}\right)$ is the TEC value of the considered grid point *(i,j)* and d_i is the distance between point *(i+1,j)* and point *(i,j)*. Similar terms are used in Eq. (2) in which $TEC\left(GP_{i,j+1}\right)$ is the easterly point of the grid with respect to *(i,j)*. Given the density of the considered networks and the division in sub regions reported in the previous section, the binning of the grid points has been set to 1° latitude x 1° longitude for the East SEA, West SEA and Brazilian equatorial regions, while 0.5° latitude x 0.5° longitude for the Brazilian crest region.

B. TIDs detection

Algorithms to detect the presence of TIDs have been run on TEC maps obtained at every 5-minute interval, over the regions of interest for the two quietest days, accordingly to what is described above. The networks used to produce TEC maps are those described in Figure 1 and Figure 2. TEC data was detrended by subtracting a 4-hour running average in each latitude-longitude bin, which is the same as that of the TEC maps. The running average window of 4 hours was chosen in order to detect the variations due to both LSTIDs and MSTIDs. The detrended TEC thus contained only its perturbation components and was used to generate the temporal latitudinal and longitudinal TEC perturbation profiles at the corresponding longitudinal and latitudinal sectors, respectively. As this study was concerned only with the TEC variations associated with TIDs, increases/decreases in the amplitude of the TEC perturbations above/below a threshold of 0.2 TECU were used to detect the presence of TIDs. The propagation parameters (period, horizontal drift velocity and horizontal wavelength) of the detected TIDs have been estimated based on the assumption that TIDs propagate as a plane wave. The time lag was determined by running the cross correlation function on the TEC perturbation profiles and the distance estimated from the latitude and longitude values of the observed TEC perturbations. The apparent velocity was then calculated dividing the distance by the time lag. To determine the period of the TEC perturbations, a Fast Fourier Transform (FFT) was then performed on the TEC perturbation temporal profiles. The values for the horizontal wavelength were determined from the values of the velocity and time period. In this study, MSTIDs are defined as TEC perturbations that satisfy the following criteria:

(1) The TEC perturbation has an amplitude exceeding 0.2 TECU;
(2) The horizontal wavelength of the TEC perturbation is smaller than 600 km;
(3) The period of the TEC perturbation is lower than 60 min.

The LSTIDs are defined as TEC perturbations that satisfy the following criteria:

(1) The TEC perturbation has an amplitude exceeding 0.2 TECU;
(2) The horizontal wavelength of the TEC perturbation is larger than 1,000 km;
(3) The period of the TEC perturbation is greater than 60 min.

After validating the algorithm on mid-latitude data by comparing the results with those reported in [24] (not shown here for the sake of conciseness), it was applied on TEC maps generated over SEA and Brazil.

C. Scintillations occurrence

For what concerns ionospheric scintillation, we concentrated our analysis on the amplitude scintillation index (S4) calculated by a given receiver every minute for each satellite in view. The considered scintillation receivers provide S4 calculated on GPS L1 every minute. To minimize the effect of multipath mimicking actual ionospheric scintillation, an elevation angle

(α_{elev}) mask of 30° has been applied. The S4 index is projected to the vertical, with the aim to minimize the effect of the geometry of the GPS receivers network. Such verticalization is performed by deriving S_4^{vert} according to the following formula:

$$S_4^{vert} = S_4^{slant} / (F(\alpha_{elev}))^{\frac{p+1}{4}} \qquad (3)$$

where S_4^{slant} is the amplitude scintillation index directly measured by the receivers, p is the phase spectral slope and $F(\alpha_{elev})$ is the obliquity factor introduced by [25], defined as:

$$F(\alpha_{elev}) = \frac{1}{\sqrt{1-\left(\frac{R_E \cos \alpha_{elev}}{R_E + H_{IPP}}\right)^2}} \qquad (4)$$

In Eq. (4), R_E is the Earth's radius and H_{IPP} is set to 350 km, where *IPP* stands for ionospheric piercing point.

The assumptions behind the verticalization are:

- weak scattering regime, which allows the use of formula (31) of [26] to derive equation (3).
- single phase screen approximation, which allows writing the exponent of the obliquity factor in formula (3) as $\frac{p+1}{4}$.

As the scintillation receivers in the IRIS/IBISCO network do not directly measure the value of the phase spectrum p, some extra assumptions are needed. By following the recommendations of [16], we adopted the same value of p=2.6 introduced by [27], which makes the exponent in equation (3) equal to 0.9. A detailed discussion about the validity and perils of such assumptions is given in [28]. Hereafter, we refer to S_4^{vert} as S_4.

D. TEC mapping method sensitivity

The sensitivity of TEC and TEC gradients mapping to the density of the GNSS network is discussed to assess the reliability of the adopted method. The TEC maps obtained with the GNSS stations from the IBGE-RBMC network covering the southern crest region have been used as the «ionospheric truth». Different numbers of fictitious stations located on a regular grid have been used to create the synthetic networks. In particular, five synthetic networks have been considered, with 4, 16, 36, 64 and 100 stations. For each synthetic network, the position of IPPs has been calculated considering the actual position of the GPS satellites, and the corresponding TEC value is sampled from the truth map obtaining the synthetic values of TEC. Such values are finally used to obtain a synthetic map of TEC (through their interpolation) and TEC gradients (according to the method described in section II.B). Synthetic maps have the same resolution and boundaries of the truth ones. An example of the synthetic receivers' location, of the position of the corresponding synthetic IPPs' (calculated on 10 March 2015 at 06 AM local time) with respect to the grid points of the ionospheric truth map is provided in Figure 3.

To provide a figure of merit, differences between truth and synthetic maps of TEC, ΔTEC_{N-S} and ΔTEC_{E-W} have been evaluated for the following days:

- 10 March 2015 at 06AM/PM
- 30 December 2015 at 06AM/PM

Such days have been selected as they are representative of the equinoctial and solsticial conditions.

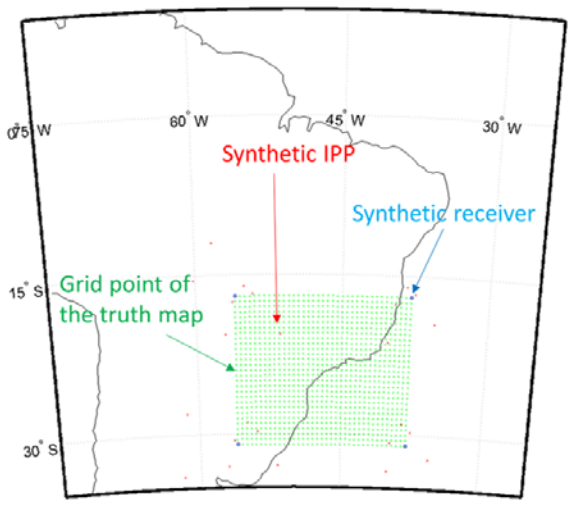

Fig. 3. Example of synthetic receivers' location (4 blue dots), position of the synthetic IPP's (red dots) and of the grid point of the ionospheric truth map (green points).

Results of the sensitivity analysis on 30 December 2015 at 06 PM are provided in Figure 4 as an example. The first, second and third rows of Figure 4 report the histograms of the point by point differences between the truth and synthetic maps considering 3 different synthetic networks made up of 4, 36 and 100 fictitious stations, respectively. First column in Figure 4 shows the differences (ΔTEC) between TEC_{true} and TEC_{synt} while the second and third column report the differences ΔTEC_{N-S} and ΔTEC_{E-W}, respectively.

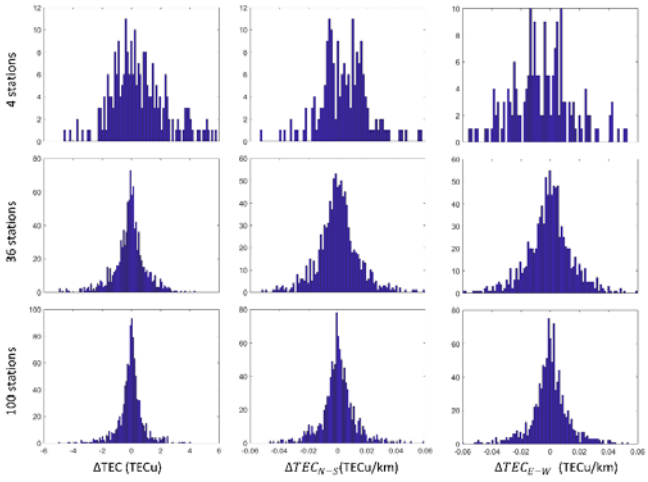

Fig. 4. ΔTEC (left column), ΔTEC_{N-S} (middle column) and ΔTEC_{E-W} (right column) considering 3 different synthetic networks including 4 (top row), 36 (middle row) and 100 stations (bottom row).

To provide an overview of such results, Figure 5 reports the standard deviation (SD) of the ΔTEC (top), ΔTEC_{N-S} (middle) and ΔTEC_{E-W} as a function of the number of the synthetic stations. Different colours correspond to the 4 considered periods, according to the legend. At equinox, the SD is

generally larger than at solstice, being up to about 5 times larger at 18 LT. The figure clearly illustrates that the SD saturates when the number of stations increases, indicating that few tenths of receivers can be sufficient to efficiently cover regions like the one under consideration. Such information is crucial to support the Biomass mission, because it provides a quantitative assessment of the GNSS receivers necessary to provide a realistic picture of the local ionosphere. The sensitivity exercise has been applied on the Brazilian southern crest because this sector includes many more stations than the SEA region.

IV. Results and Discussion

The results of the analysis conducted according to the method described in the previous section are here given in the form of slice plots and graphs to describe the monthly variation of the ionospheric climate in the regions under investigation.

A. SEA region – TEC spatial gradients

Figure 6 shows the monthly variation of the mean of the absolute value of the TEC gradients at 06 AM and 06 PM along the N-S direction over West (panels a and b) and East (panels c and d) SEA. In the figure, also the 1σ (grey), 2 σ (green) and 3 σ (red) variations are reported. To obtain such values, a window of 1 hour centred around 06 AM and 06 PM local time is considered. Over both sectors, the equinoxes result highly variable at both considered times, even if in the West SEA the larger variance is found in December at 06 AM, implying the simultaneous presence of irregularities of different scale sizes during the equinoctial months and around the December solstice. To complete the picture provided by Figure 7 shows the monthly variation of the mean of the absolute value of the TEC gradients at 06 AM and 06 PM along the E-W direction over West (panels a and b) and East (panels c and d) SEA. Similarly to the N-S gradients, in both SEA regions the larger gradients and variability are found in the equinoctial months. Also in this case, the variability peak is found in December over West SEA at 06 AM.

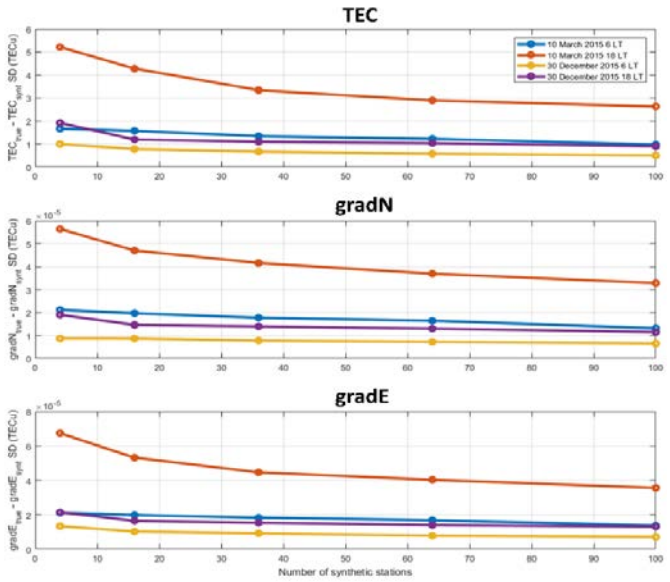

Fig. 5. Standard deviation (SD) of the TEC (top), ΔTEC_{N-S} gradient (middle) and ΔTEC_{E-W} gradient (bottom) differences as a function of the number of the synthetic stations. Different colors correspond to the 4 considered periods, according to the legend.

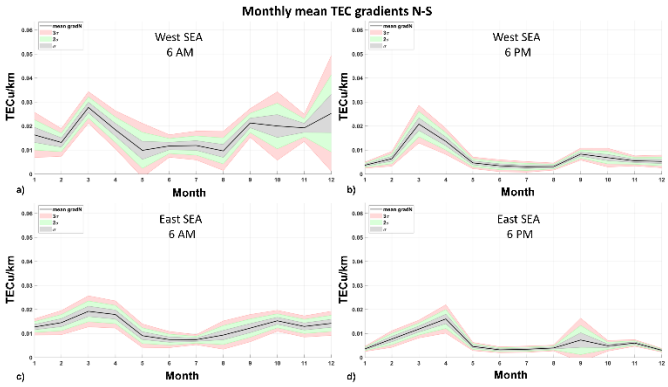

Fig. 6. Monthly variation of the hourly mean TEC gradients (North-South direction) over West (a, b) and East (c, d) SEA. Panels a and c refer to 06 AM, panels b and d to 06 PM.

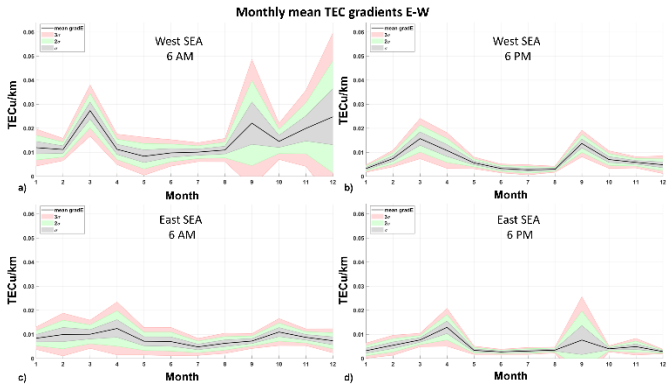

Fig. 7. Monthly variation of the hourly mean TEC gradients (East-West direction) over West (a, b) and East (c, d) SEA. Panels a and c refer to 06 AM, panels b and d to 06 PM.

Figure 8 and Figure 9 show the slice plots of the monthly variation of the TEC mean gradients and their standard deviations along the North-South and the East-West direction at 06 AM and 06 PM under West and East SEA. The pictures highlight the seasonal variation, clearly identifying the equinoctial months as the most disturbed. It is interesting to notice the change of sign around 20°N, over both West and East SEA. It is identified by a plateau (mean TEC gradients around 0 TECU) that separates the region characterized by positive gradients from the region characterized by negative gradients. As the dip equator is located at 7.5° N, the gradients mapping confirms the presence of the EIA crest around 20°N and the TEC positive and negative slopes before and after the plateau. The West SEA presents a larger variability of the gradients in the proximity of the dip equator. From the standard deviations, the variability of the meridional gradients results to be larger around the dip equator and the EIA northern crest over the West SEA. The zonal gradients over West SEA results positive and negative in the different longitudinal sectors observed. Over West SEA, the equinoctial and December months are clearly identified as the best candidates to host the greater zonal gradients. In the same sector, the signatures of the crest and of the dip equator are recognisable. Over East SEA, the zonal gradients are very low and evenly distributed, the crest signature is visible just between 15°-20°N and at the highest

longitude. The variability shown by the standard deviation is quite low over both West and East SEA, with a slight enhancement over the dip equator and within the crest.

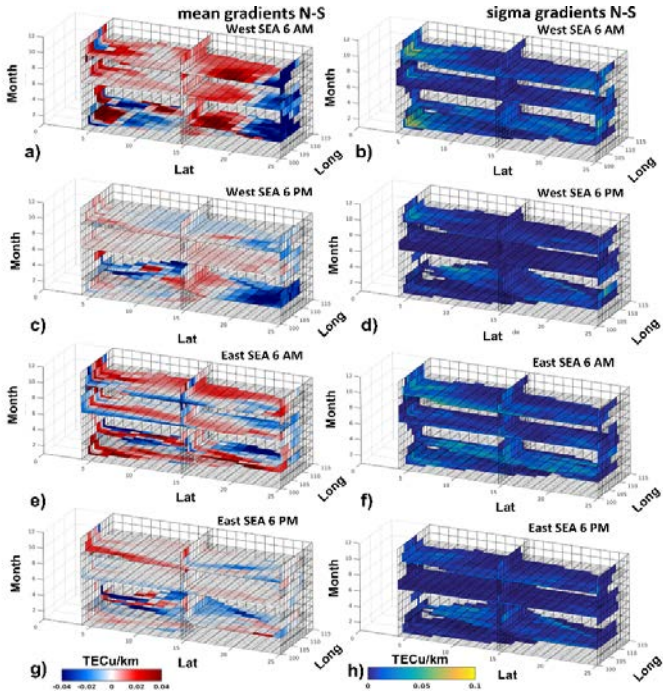

Fig. 8. Slice plots of the monthly variation of the TEC mean gradients (a,c, e, g) along the North-South direction and their standard deviations (b,d,f,h) over West (a,b,c,d) and East (e,f,g,h) SEA at 06 AM and 06 PM.

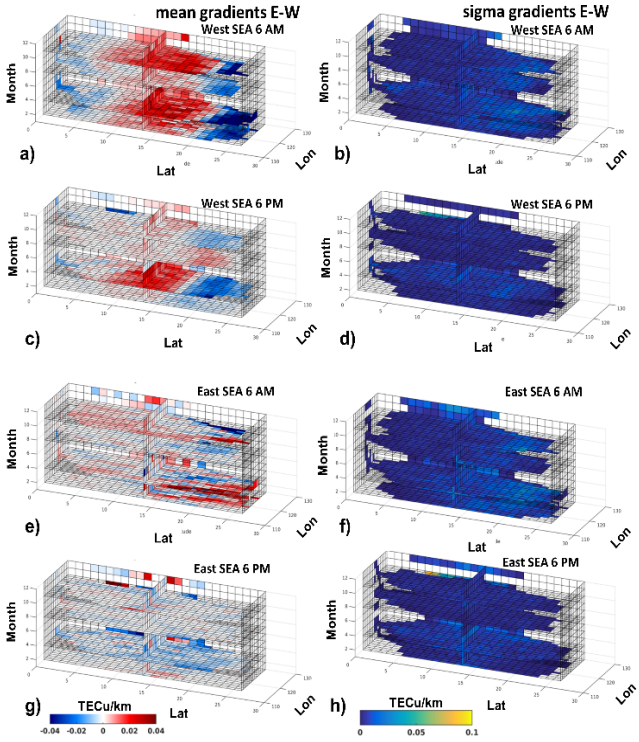

Fig. 9. Slice plots of the monthly variation of the TEC mean gradients (a,c, e, g) along the East-West direction and their standard deviations (b,d,f,h) over West (a,b,c,d) and East (e,f,g,h) at 06 AM and 06 PM.

B. *SEA region – Scintillations*

The monthly variation of the scintillation occurrence has been produced over the East and West SEA, covering the region between the dip equator and the southern EIA crest, as well as the region of the dip equator and the two EIA crests, respectively (Figure 10). The occurrence has been sorted according to three levels of amplitude scintillations: S_4>0.1, S_4>0.25; S_4>0.7 and by considering a 1-hour window centred at 06 AM and 06 PM LT.

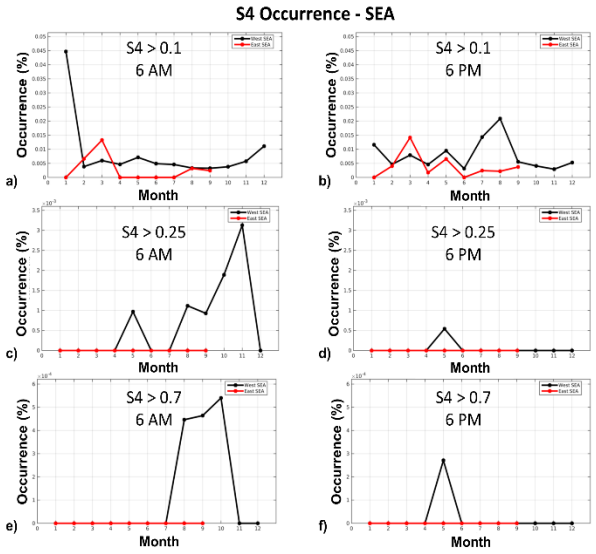

Fig. 10. Monthly variation of the S4 occurrence above three levels of scintillation over East (red) and West (black) SEA. Left plots refer to 06 AM, while right plots to 06 PM.

The seasonal behaviour shows how the equinoctial maxima characterize all the levels of scintillations (from weak to strong scattering regimes). A gap in the data from October to December 2015 and on January 2016 do not allow to characterize the seasonal variation in the East SEA region.
The monthly variation of the scintillation occurrence for S_4>0.1 West and East SEA is shown in the slice plots of Figure 11. Even though the seasonal scenario over East SEA is not completed because of the data gap from October to December 2015 and on January 2016, the figure shows the presence of scintillations in the spring equinox at both 06 AM and 06 PM in the East SEA region. The seasonal behaviour in the West SEA shows a fairly even distribution of scintillation all year long during both time intervals

C. *SEA region – TIDs*

The TIDs detection algorithms have been run on TEC maps used for TEC gradients analysis as described in Section 2.2.
It was observed that none of the analysed days revealed the presence of LSTIDs over these regions. It is well known that the LSTIDs are generally observed during geomagnetic storms, as these are mainly generated by Joule heating produced from intense particle precipitation in the auroral and sub-auroral regions [13], [14]. All the days analysed in this study are geomagnetically quiet and therefore not associated with any disturbances, which agrees with the absence of LSTIDs.

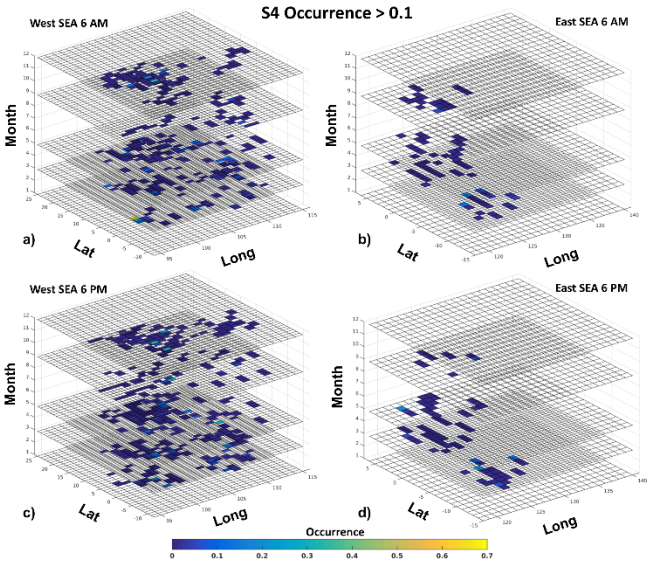

Fig. 11. Slice plots of the monthly variation of the S4 occurrence above 0.1 over West and East SEA.

An MSTID was detected only on one day. The estimated parameters are shown in Table 1.

TABLE 1
APPARENT VELOCITY, TIME PERIOD AND WAVELENGHT OF THE MSTID DETECTED IN THE SEA REGION ON 30 AUGUST 2015

Day number	Apparent velocity (km/s)	Time period (minutes)	Wavelength (km)
242/2015	0.0722	45	195

D. Brazil – TEC spatial gradients

Panels a and b of Figure 12 show the monthly variation of the mean of the absolute value of the TEC gradients along the N-S direction under the EIA southern crest. The maxima are located in March and between September and October, confirming a higher degree of ionospheric disturbance during the equinoctial months. Moreover, the gradients are generally larger around 06 PM than around 06 AM. It is interesting to notice the intense scattering of the gradients observed in May and June at 06 AM. Such feature implies the simultaneous presence of irregularities of different scale sizes during such months.

Panels c and d of Figure 12 show the monthly variation of the mean of the absolute value of the TEC gradients along E-W direction under the EIA southern crest. At 06 PM (panel d), the maxima are found during the equinoxes (on March and September) and the minima occur in July and between December and January. This is exactly the same pattern found for the meridional gradients in the same time interval. At 06 AM (panel c), again three maxima are present: March, June and September. Also, in this case, the strongest scattering of the gradients is found during equinoxes and winter, indicating the presence of different scale sizes of the ionospheric structuring also along the East-West direction.

Panels a and b of Figure 13 show the monthly variation of the mean of the absolute value of the TEC gradients along the N-S direction over the dip equator. In the figure, plots have been obtained considering a 1-hour window centred at 06 AM (panel a) and 06 PM (panel b).

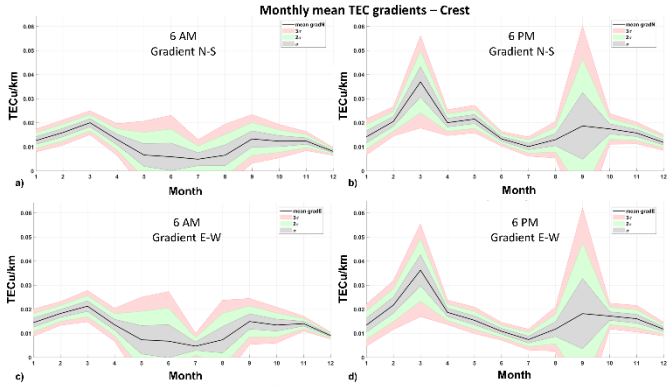

Fig. 12. Monthly variation of the hourly mean TEC gradients along North-South (a,b) and East-West (c,d) directions under the EIA southern crest at 06 AM (a,c) and at 06 PM (b,d)

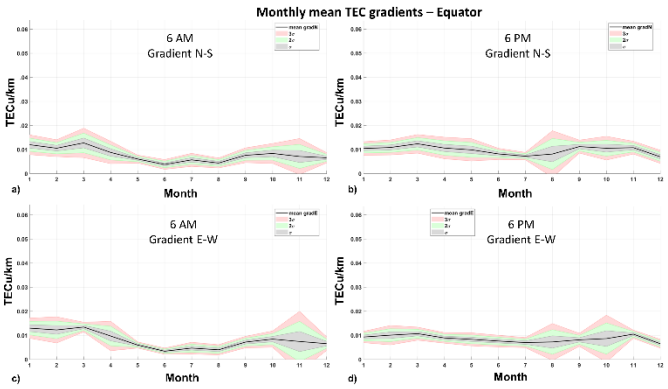

Fig. 12. Monthly variation of the hourly mean TEC gradients along North-South (a,b) and East-West (c,d) directions under the dip equator at 06 AM (a,c) and at 06 PM (b,d).

Comparing these panels to the corresponding ones of Figure 12, it is evident the lower values of the gradients over the dip equator with respect to those recorded under the southern crest of the EIA. The main differences arise at 06 PM. At 06 AM, again three maxima are present: March, July and November. At 06 PM, the largest variability of the ionospheric structuring close to the equator is found in August, and two maxima are found in March and in October, even if less pronounced than in the case of 06 AM. Panels c and d of Figure 13 report the same as panels a and b, but for the zonal gradient. In this case, again the values are generally lower than those under the crest. At 06 AM, larger variability gradients are found in November and between January and April. Minimum values and variability are found in the winter time. At 06 PM, the larger variability of the gradients is found in August and October.

Figure 14 and Figure 15 show the 3D representation of the monthly variation of the TEC mean gradients (left panels) and their standard deviations (right panels) along the North-South direction (left) and East-West direction (right) under the dip equator (Figure 14) and around the EIA southern crest (Figure 15) at 06 AM (a-d) and at 06 PM (e-h).

The figures highlight how the meridional TEC gradients increase during the equinoctial months (March and October) and present a high degree of variability of the ionospheric structuring. It is interesting to notice the change of sign (negative gradients) around the same months in the region of

the crest closer to the dip equator (located around -9° N), corresponding to the highest degree of variability shown by the standard deviation. The zonal gradients show a larger variability in the sign, but confirm the presence of the ionospheric irregularities of different scale sizes mainly in March and also in October. The change of sign (positive gradients) around the same months in the region of the crest closer to the dip equator (located around -9° N) appears similar to the one identified in the N-S gradients.

In the dip equator (Figure 14), the monthly variation of the meridional gradients shows significant values but with a meaningfully lower variability with respect to those observed in the crest. The E-W gradients show the same scenario; gradients comparable with those found under the crest (Figure 15), but with a significantly lower variability. This means that around the dip equator the ionospheric structuring along the East-West and along the N-S direction is less variable than in the crest.

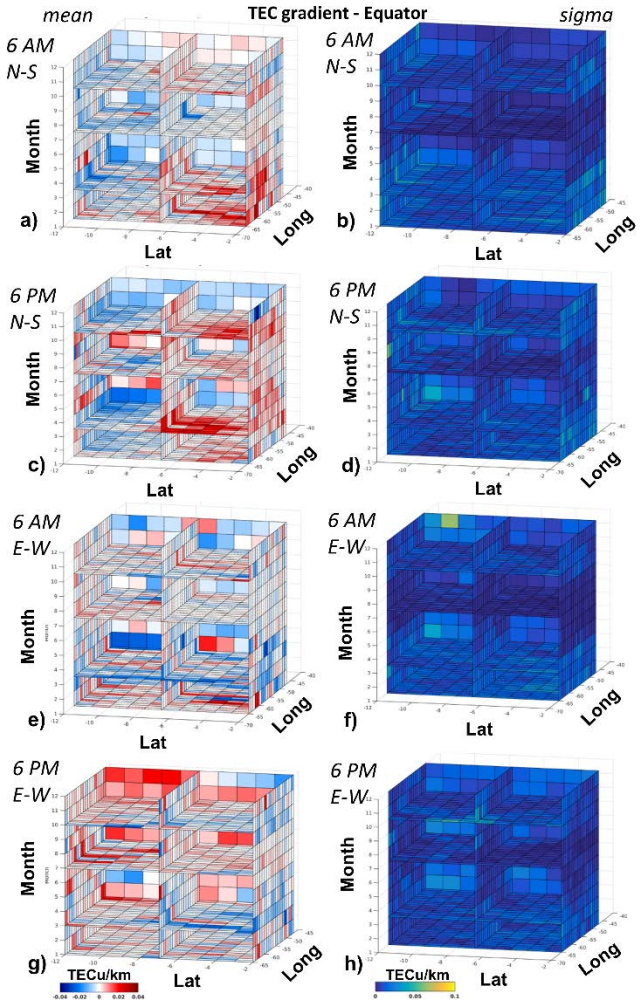

Fig. 13. Slice plots of the monthly variation of the TEC mean gradients (a,c,e,g) along the North-South direction and East-West direction and their standard deviations (b,d,f,h) over the dip equator at 06 AM and 06 PM.

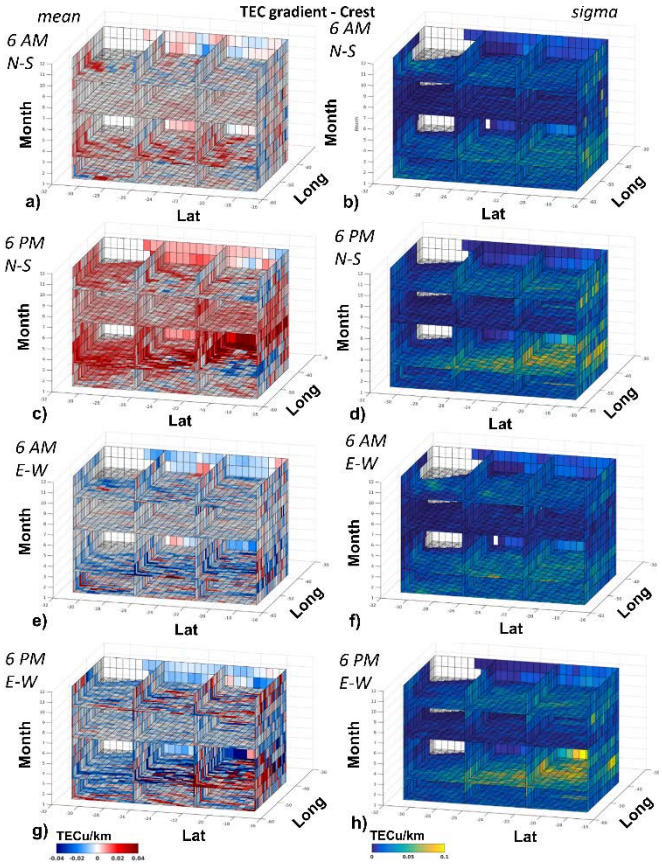

Fig. 14. Slice plots of the monthly variation of the TEC mean gradients (a,c,e,g) along the North-South direction and East-West direction and their standard deviations (b,d,f,h) over the EIA southern crest at 06 AM and 06 PM.

E. Brazil – Scintillations

The monthly variation of the S_4 occurrence for the three levels of amplitude scintillation (S_4>0.1, S_4>0.25, S_4>0.7), considering the two 1-hour windows centred at 06 AM and 06 PM, is given in Figure 16. The seasonal behaviour shown in Figure 16 highlights that, on a statistical base, there is no occurrence of strong scintillation events at 06 AM and 06 PM in neither the crest nor the dip equator (Figure 16 e-f). The equinoctial maxima characterize mainly the moderate scattering regimes of the crest region (Figure 16, middle plots) and the weak scattering regime of the equatorial region (Figure 16 a-b). The equatorial region is also characterized by an increase of the occurrence in June for the weak scattering regime (Figure 16, panels a-b) at both 06 AM and 06 PM, and for the moderate scattering regime at 06 AM (Figure 16, panel c). Comparing the seasonal behaviour of the weak scintillation (S4>0.1) occurrence within the crest and in the dip equator (Figure 17), the manifestation results similar in the two regions.

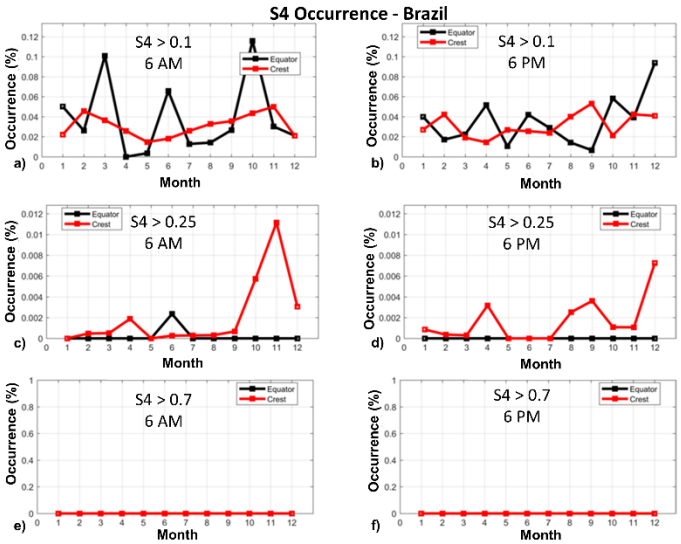

Fig. 15. Monthly variation of the S4 occurrence above three levels of scintillation under the EIA southern crest (red) and around the dip equator (black). Left panels refer to 06 AM, right panels to 06 PM.

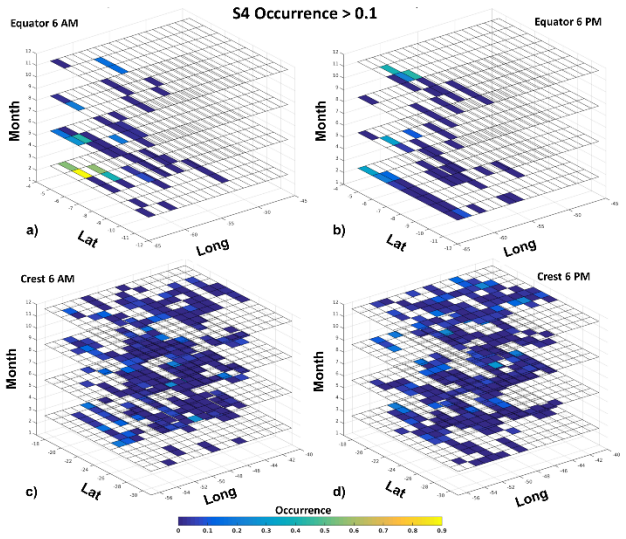

Fig. 16. Slice plots of the monthly variation of the S4 occurrence above 0.1 in the dip equator (top) and within the EIA southern crest (bottom). Left panels refer to 06 AM, right panels to 06 PM.

F. Brazil – TIDs

Algorithms to detect the presence of TIDs were run on TEC maps obtained at every 5 minutes interval, over the equatorial and anomaly crest regions in Brazil (see Section 2.2 for the method). The TEC maps for the equatorial regions covered a spatial range of -12.0°N to -2.0°N in IPP latitude and -65.0°E to -47.0°E in IPP longitude with a 1° resolution, while over the anomaly crest regions they covered a spatial range of -31.0°N to -17.0°N in IPP latitude and -56.0°E to -38.0°E in IPP longitude with a 0.5° resolution.

It was observed that none of the analysed days revealed the presence of LSTIDs over these regions, as expected during geomagnetically quiet conditions.

The MSTIDs were detected on one day over the crest and on two days over the equatorial region during the year 2015. The main characteristics of the MSTIDs observed over the crest and equatorial region are summarised in Table 2.

TABLE 2.
THE APPARENT VELOCITY, PERIOD AND WAVELENGTH OF THE DETECTED MSTIDS.

Day number	Apparent velocity (km/s)	Time period (minutes)	Wavelength (km)	Region
018	0.124	14	106	Crest
226	0.0833	25	125	Equator
329	0.1852	45	500	Equator

V. CONCLUSIONS

The TEC gradients characterizing the low latitude ionosphere can degrade the quality of the imaging that the P-band SAR on board the future Biomass ESA mission will provide. The original approach proposed in this paper offers a climatological picture of the low-latitude ionosphere properly customized to provide the information needed for the Biomass mission operational purposes. Such information cannot be entirely derived from global models of the ionosphere. This is the reason why this work is proposed as a valuable contribution to the regional characterization of the ionospheric impact on remote sensing.

Space weather introduces a high level of ionospheric unpredictability in the SEA and Brazilian regions due to the complex dynamics occurring in proximity of the EIA. Indeed, TEC variations and scintillation occurrence can be very different from case to case, often being associated with very fine structuring of the ionospheric plasma. This means that a reliable assessment of the ionospheric scenario, even during quiet times, must rely on data driven representation. Indeed, our statistical analysis of the TEC gradients and of scintillations reveals:

- An important distinction between the meridional TEC variation and the zonal variation in both regions under investigation;
- A clear definition of the role of EIA crests in hosting the ionospheric irregularities;
- Peculiar characteristics of the low-latitude ionosphere at the Biomass orbital passes (06 AM, 06 PM);
- The contribution of MSTIDs to TEC variations is minor but not negligible during quiet time.

Our assessment of the sensitivity of the method adopted to calculate both TEC and corresponding gradients to the number of the receivers in the network indicates that few tenths of receivers can be sufficient to provide a reliable climatology over regions like the one considered in Brazil.

REFERENCES

[1] .*Report for Mission Selection: Biomass*, ESA SP-1324/1 (3 volume series), European Space Agency, Noordwijk, The Netherlands.

[2] S. Quegan, N. C. Rogers, K. P. Papathanassiou, J. S. Kim, R. Scheiber, F. Rocca, S. Tebaldini, and L. Iannini. "Ionospheric mitigation schemes and their consequences for Biomass product quality," European Space Agency, Paris, France (2012).

[3] M. C. Kelley, "The Earth's Ionosphere Plasma Physics and Electrodynamics", *International Geophysics Series*, vol. 43, Academic Press, San Diego, California, 1989.

[4] E.V. Appleton, "Two anomalies in the ionosphere", *Nature*, 157 (1946), p. 691.

[5] R. A. Heelis, "Electrodynamics in the low and middle latitude ionosphere: A tutorial", *J. Atmos. Sol. Terr. Phys.*, 66, 825–838, 2004.

[6] N. Balan, and G. J. Bailey, "Equatorial plasma fountain and its effects: Possibility of an additional layer", *J. Geophys. Res.*, 100(A11), 21,421–21,432, 1995, doi:10.1029/95JA01555.

[7] R. F. Woodman, "Vertical drift velocities and east-west electric fields at the magnetic equator," *J. Geophys. Res*., 75(31), 6249–6259, 1970, doi:10.1029/JA075i031p06249.

[8] S. Chatterjee, S. K. Chakraborty, B. Veenadhari, and S. Banola, "A study on ionospheric scintillation near the EIA crest in relation to equatorial electrodynamics", *J. Geophys. Res. Space Physics*, 119, 1250–1261, 2014, doi:10.1002/2013JA019466.

[9] S. Basu, et al., "Scintillations, plasma drifts, and neutral winds in the equatorial ionosphere", *J. Geophys. Res.*, 101, 26,783–26,795, 1996.

[10] M. Mendillo, "Storms in the ionosphere: Patterns and processes for total electron content." *Reviews of Geophysics* 44.4, 2006.

[11] C. O. Hines, "Internal atmospheric gravity waves at ionospheric heights", *Can. J. Phys.*, 38, 1441–1481, 1960, doi:10.1139/p60-150.

[12] M. Hernández-Pajares, J. M. Juan, and J. Sanz, "Medium-scale traveling ionospheric disturbances affecting GPS measurements: Spatial and temporal analysis", *J. Geophys. Res*., 111, A07S11, 2006, doi:10.1029/2005JA011474.

[13] K. Hocke, and K. Schlegel, "A review of atmospheric gravity waves and traveling ionospheric disturbances: 1982–1995", *Ann. Geophys*., 14, 917–940, 1996.

[14] R. D. Hunsucker, "Atmospheric gravity waves generated in the high latitude ionosphere: A review", *Rev. Geophys.*, 20, 293 – 315, 1982.

[15] L. Spogli, C. Cesaroni, D. Di Mauro, M. Pezzopane, L. Alfonsi, L., Musicò, E., ... and N. Linty, "Formation of ionospheric irregularities over Southeast Asia during the 2015 St. Patrick's Day storm", *J. Geophys. Res.Space Physics*, 121, 12,211–12,233, doi:10.1002/2016JA023222, 2016.

[16] A. W. Wernik, J. A. Secan, E. J. Fremouw, "Ionospheric irregularities and scintillation", *Advances in Space Research*, 31(4), 971-981, 2003.

[17] A. W. Wernik, L. Alfonsi, and M. Materassi. "Ionospheric irregularities, scintillation and its effect on systems", *Acta Geophysica Polonica* 52, no. 2 (2004): 237-249.

[18] G. Povero, L. Alfonsi, L. Spogli, D. Di Mauro, C. Cesaroni, F. Dovis, R. Romero, M. Le Huy, P. Abadi, V. La The, N. Floury, "Ionosphere Monitoring in South East Asia in the ERICA study", *NAVIGATION*, 2017, Vol. 64, Issue 2, pp. 273-287, ISSN: 2161-4296, doi:10.1002/navi.194

[19] L. Ciraolo, F. Azpilicueta, C. Brunini, A. Meza, and S.M. Radicella, "Calibration errors on experimental slant total electron content (TEC) determined with GPS", *Journal of Geodesy*, 2007, 81(2), 111-120.

[20] C. Cesaroni, L. Spogli, L. Alfonsi, G. De Franceschi, L. Ciraolo, J. F. G. Monico, ... and B. Bougard, "L-band scintillations and calibrated total electron content gradients over Brazil during the last solar maximum, " *Journal of Space Weather and Space Climate*, 2015, 5, A36.

[21] M. P. Foster and A. N. Evans, "An Evaluation of Interpolation Techniques for Reconstructing Ionospheric TEC Maps", *IEEE Trans. Geosci. Remote Sens.*, 46(7), 2153–2164, doi:10.1109/TGRS.2008.916642, 2008.

[22] A. Okabe, B. Boots, and K. Sugihara, "Nearest neighbourhood operations with generalized Voronoi diagrams: a review", *Int. J. Geogr. Inf. Syst.*, doi:10.1080/02693799408901986, 1994.

[23] D. T. Lee, and B. J. Schachter, "Two algorithms for constructing a Delaunay triangulation", *Int. J. Comput*. Inf. Sci., 9(3), 219–242, doi:10.1007/BF00977785, 1980.

[24] C. Cesaroni, L. Alfonsi, M. Pezzopane, C. Martinis, J. Baumgardner, J. Wroten, M. Mendillo, E. Musicò, M. Lazzarin, and G. Umbriaco, "The first use of coordinated ionospheric radio and optical observations over Italy: Convergence of high and low latitude storm-induced effects?", *Journal of Geophysical Research: Space Physics*, 2017,122. https://doi.org/10.1002/2017JA024325.

[25] A. J. Mannucci, B. D. Wilson, and C. D. Edwards, "A new method for monitoring the Earth's ionospheric total electron content using the GPS global network", in *Proc. of ION-GPS*, 1993 pp. 1323-1332.

[26] C. L. Rino, "A power law phase screen model for ionospheric scintillation: Weak scatter", *Radio Sci*., 1979, 14, 1135–1145, doi:10.1029/RS014i006p01135.

[27] L. Spogli, L. Alfonsi, G. De Franceschi, V. Romano, M. H. O. Aquino, and A. Dodson, "Climatology of GPS ionospheric scintillations over high and mid-latitude European regions", *Ann. Geophys*, 2009, 27, 3429-3437.

[28] L. Spogli, L. Alfonsi, V. Romano, G. De Franceschi, G. M. J. Francisco, M. H. Shimabukuro, ... and M. Aquino, "Assessing the GNSS scintillation climate over Brazil under increasing solar activity", *Journal of Atmospheric and Solar-Terrestrial Physics*, 2013, 105, 199-206.

Lucilla Alfonsi received the M.Sc. degree in Physics from the Sapienza University of Rome and the PhD in Geophysics from the Alma Mater Studiorum – Università di Bologna, Bologne, Italy. She is expert on the investigation of ionospheric irregularities from ground based as well as from in situ measurements and on ionospheric modelling. She is the PI of the IRIS project.

Gabriella Povero received the M.Sc. degree in Electronics Engineering at Politecnico di Torino. Since 2003 she has been with Istituto Superiore Mario Boella where is responsible of the unit International Cooperation in GNSS in the Satellite Navigation Research Area. She is the PI of the IBISCO project.

Luca Spogli received MSc and PhD in physics from Roma Tre University (Italy). Since 2008, he is researcher at the Istituto Nazionale di Geofisica e Vulcanologia in the Upper Atmosphere Physics group. He is expert of ionospheric physics, modelling, data analysis and treatment techniques.

Claudio Cesaroni received M.Sc. degree in "Physics" at "Sapienza" University of Rome and PhD degree in Geophysics at the University of Bologna. Since 2015, he is researcher at Istituto Nazionale di Geofisica e Vulcanologia, working mainly on TEC calibration technique, effects of spatial and temporal gradients on GNSS signals and ionospheric models development and validation.

Biagio Forte is PhD in Geophysics, Karl-Franzens University of Graz (Austria). He is currently lecturer at the Department of Electronic & Electrical Engineering Centre for Space, Atmospheric and Oceanic Science of the University of Bath. He is expert in the physics and chemistry of the upper ionised atmosphere, plasma turbulence and instabilities, radio wave scintillation.

Cathryn N. Mitchell, PhD is Professor at the Department of Electronic & Electrical Engineering Centre for Space, Atmospheric and Oceanic Science of the University of Bath. She is expert on Satellite Navigation Systems and Signal Processing.

Robert Burston is Research Fellow at the Department of Electronic & Electrical Engineering Centre for Space, Atmospheric and Oceanic Science of the University of Bath.

Sreeja Vadakke Veettil is a Senior Research Fellow at the Nottingham Geospatial Institute of the University of Nottingham in the UK. Her research focuses on assessing the effects of space weather on GNSS receivers and positioning errors aiming to improve the modeling of scintillation and to develop mitigation tools.

Marcio Aquino is Associate Professor at the Faculty of Engineering of the University of Nottingham. He is a Geodesist with a PhD in Space Geodesy. He has worked on mitigation of ionospheric effects on Global Navigation Satellites Systems (GNSS) since 2001 and leads the Nottingham Geospatial Institute (NGI)'s research theme 'Propagation Effects on GNSS'

Virginia Klausner has a Master's degree in Physics and Astronomy from the University of Vale do Paraíba (2007), and a doctorate in geophysics at the National Observatory in Rio de Janeiro (2012). She is assistant professor at UNIVAP and her expertise is in the area of signal processing for Geosciences, with emphasis on Aeronomy and Space Geophysics.

Marcio T. A. H. Muella is associated professor in the School of Engineering and in the Institute of Research and Development (IP&D) at the UNIVAP. He earned his B.E. degree in electrical and electronic engineering from UNIVAP in 2002, his M.Sc. degree in 2004 and a Ph.D. degree in 2008 in space geophysics from National Institute for Space Research (INPE), Brazil. He works in ionospheric research where the main interest field lies in GNSS related topics, including space weather.

Michael Pezzopane is researcher at INGV since 2001. He got his Master Science in Physics at Sapienza University of Rome, Italy, and his Ph.D. in Geophysics at the University of Bologna, Italy. His main research interests are: radio wave propagation in the ionosphere, electron density irregularities at low latitudes, ionogram autoscaling, ionospheric modelling.

Alessandra Giuntini received MSc in physics from Roma Tre University (Italy) and PhD in geophysics from Bologna's Alma Mater Studiorum University (Italy). Since 2007, she is researcher at the Istituto Nazionale di Geofisica e Vulcanologia. Her expertise are in seismic location, data analysis and communication fields.

Ingrid Hunstad MSc in Physics (1993) at the University of Rome “La Sapienza”. Specialization (PhD equivalent) in Geophysics (1997) at INGV. She is researcher in the Upper Atmosphere Physics Research Unit of INGV. She is expert on GNSS systems expertise, management of the GNSS network for scintillation and TEC monitoring.

Giorgiana De Franceschi has the doctoral degree in Physics (*summa cum laude*) in December 1981 at “'Università degli Studi "La Sapienza" of Rome”. She is currently Director of Research at Istituto Nazionale di Geofisica e Vulcanologia-INGV (formerly ING). Her main research interests are the temporal/spatial modelling of the high and low latitude ionosphere. In 2017, she has been elected URSI (International Union on Radio Sciences) Commission G vice-chair.

Elvira Musicò received the M.Sc. degree in Physics from the Alma Mater Studiorum – Università di Bologna, Bologne, Italy, and the Ph.D. degree from the Sapienza University of Rome in 2014 and 2018, respectively. Since 2012, she is part of the Upper Atmosphere Physics group of INGV, involved in the study of Global Navigation Satellite System data and Interferometric SAR images.

Marco Pini received the Ph.D. degree in electronics and communications from Politecnico di Torino University. He is currently the Head of the Navigation Technologies Research Area, Istituto Superiore Mario Boella. His major research interests cover the field of baseband signal processing on new GNSS signals, multi-frequency RF front end design, and software radio receivers.

Vinh La The is PhD in Computer Engineering (Kyung Hee University, Korea), MSc in Computer Engineering (Hanoi University of Technology). He is vice director of NAVIS Centre, Hanoi University of Science and Technology and Assistant Professor at School of Information and Communication Technology, Hanoi University of Science and Technology.

Hieu Tran Trung received the Engineer Degree from the School of Information and Communication Technology of the Hanoi University of Science and technology and a PhD in Electronics and Communications Engineering from the Politecnico di Torino. He is currently working at the NAVIS Centre, Hanoi University of Science and Technology. His research activity focuses on GNSS software receivers and GNSS integrity.

Asnawi Husin received his Master of Science, from Electrical Electronic Engineering National Universtiy of Malaysia (UKM) in 2011. Since 2000, he his Permanent Researcher at Ionospheric and Telecommunication Division Space Science Center National Institute of Aeronautics and Space (LAPAN). He is active in the field of ionospheric space weather, processing and analyzing GNSS and ionosonde data.

Sri Ekawati received the B.S and M.S in Physics from Padjadjaran University in 2005 and from Bandung Institute of Technology (ITB) in 2014. Since 2006, she is a government employee for Space Science Center, LAPAN as Ionospheric and Magnetospheric Researcher.

Charisma Victoria de la Cruz-Cayapan has a Bachelor and a Master of Science in Geodetic Engineering, Geomatics from the University of the Philippines and a Specializing Master in Navigation and Related Applications (GNSS) from the Politecnico di Torino. She is Engineer at National Mapping and Resource Information Authority.

Mardina Abdullah. She is Professor in the Department of Electrical, Electronic & Systems Engineering, Space Science Centre (ANGKASA) of UKM. She is expert on Ionospheric prediction and irregularities, Space weather impact on GPS, GPS satellite error mitigation.

Noridawaty Mat Daud is Research Officer at Universiti Kebangsaan Malaysia (UKM), Space Science Centre (ANGKASA).